Heliyon 8 (2022) e10941

Contents lists available at ScienceDirect

Heliyon

journal homepage: www.cell.com/heliyon

Research article

Multiparameter sensor based on micro/nano-structured optical fiber and composites

Chi Liu [a,b], Yue Feng [a,b], Xin Liu [b,c], Yue Yuan [b,c], Yunqiang Li [b,c], Tao Shen [a,b,c,*]

[a] Key Laboratory of Engineering Dielectrics and Its Application, Ministry of Education, Harbin University of Science and Technology, Harbin, 150080, China
[b] Heilongjiang Province Key Laboratory of Laser Spectroscopy Technology and Application, Harbin University of Science and Technology, Harbin 150080, China
[c] Heilongjiang Province Key Laboratory of Quantum Control, Harbin University of Science and Technology, Harbin 150080, China

GRAPHICAL ABSTRACT

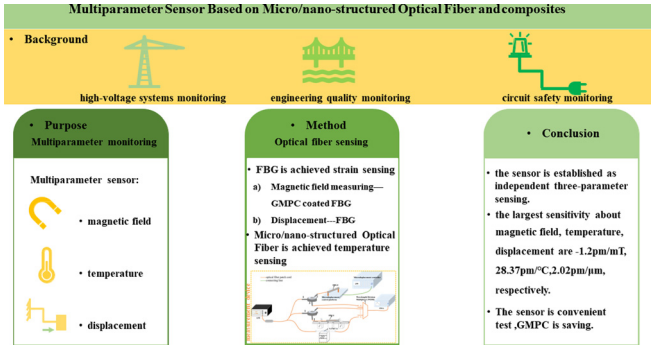

ARTICLE INFO

Keywords:
Optical fiber sensor
Three parameter measurement
Micro/nano-structured optical fiber
Fiber Bragg gratings (FBG)
Giant magnetostrictive particle composite (GMPC)

ABSTRACT

In this paper, an optical fiber sensor is realized with multi-parameter measurement, including magnetic field, temperature and displacement. Then, the implementation of the three-parameter independent measurement was performed. Among of them, one of fiber Bragg gratings (FBG) is coated giant magnetostrictive particle composite (GMPC) to measure the magnetic field, another FBG is used to measure displacement, and a micro-nano fiber structure of single mode fiber (SMF)-tapering seven core fiber (T-MCF-7)-SMF (S-TM7-S) is applied to measure temperature. Further, the GMPC concentration with the best sensitivity and the best seven-core fiber length were finally selected to form the sensing unit for simultaneous detection of the three parameters. The optical fiber sensor has potential applications for measuring magnetic field environments and system temperatures in high-voltage systems, engineering quality monitoring, as well as circuit safety monitoring.

1. Introduction

Since the advent of low-loss optical fibers in the 1970s, the research has become increasingly developed on application fields of optical fibers [1, 2, 3]. Notably, optical fibers and their composite structures have been widely used to monitor various parameters in the field of optical fiber sensing, such as: magnetic field, temperature, strain, displacement, acoustic vibration, etc. [4, 5, 6, 7], which is applied to

* Corresponding author at: Key Laboratory of Engineering Dielectrics and Its Application, Ministry of Education, Harbin University of Science and Technology, Harbin, 150080, China.
E-mail address: taoshenchina@163.com (T. Shen).

https://doi.org/10.1016/j.heliyon.2022.e10941
Received 20 April 2022; Received in revised form 20 June 2022; Accepted 29 September 2022

construction and engineering health monitoring, power system monitoring and so on [8, 9]. Among, in the field of power system monitoring, optical fibers possess many unique advantages versus other transmission media, such as: small size, light weight, anti-extreme environment, low-loss long-distance transmission, anti-electromagnetic interference, etc.

However, the working environment of the power system is extremely complicated. For example, in the high-voltage transmission line of the power system, it is easy to cause the line to dancing, further, causing displacement due to the influence of weather and extreme environment. Equally, the temperature in the power system itself will also affect the monitoring of the power system. Moreover, the high temperature may cause serious accidents such as fire [10]. Therefore, the simultaneous monitoring of temperature and displacement is very important in the process of magnetic field monitoring in power systems. Moreover, it is very necessary to use optical fiber sensing to realize multi-parameter measurement of magnetic field, temperature and displacement when conducting research on optical fiber magnetic field sensing.

In the existing optical fiber sensors, different optical fiber structures have different measurement principles, such as: fiber grating-based sensing, surface plasmon resonance sensing, fiber-optic interference sensing, etc. [4, 6, 11, 12].

Indeed, at present, with the continuous development of the field of optical fiber sensing, the functions that can be realized by optical fiber sensors continue to increase, and the optical fiber dual-parameter and multi-parameter sensing has become a research hotspot. In 2017, Tong Z et al. proposed an optical fiber sensor that measure temperature and refractive index simultaneously. The sensor adopts few-mode optical fiber and spherical structure, which can realize dual-parameter monitoring of temperature and refractive index [13]. In the same year, Yong Z et al. proposed an interferometer that can achieve high sensitivity to temperature and magnetic fields. The fiber structure of the sensor is based on hollow-core fibers [14]. Also, in this year, Li C et al. used four-core optical fiber and fiber grating to realize the sensor for three-parameter measurement of temperature, humidity and refractive index [15]. In 2018, Zhang X et al. mentioned a temperature and strain monitoring sensor based on FP interferometer and FBG [16]. In 2019, Gao X et al. realized an optical fiber sensor based on few-mode fiber and FBG with simultaneous monitoring of temperature and stress [17]. In 2020, the A.G. Leal-Junior presents a fiber Bragg grating (FBG) array immersed in magnetorheological (MR) fluid for simultaneous evaluation of magnetic field strength and position of a magnetic field sensor, and analyzes the effect of temperature on the sensor [18]. In 2021, Zhan B et al. researched a dual-FBG-based sensor that can demodulate temperature and magnetic field, and eliminate the effect of temperature through the matrix method to enhance the accuracy of magnetic field measurement [19]. In 2021, Zhang W et al. used a thin polarization-maintaining fiber and a coupler to form a sensing structure. And then, the polarization-maintaining fiber and a polarizer were connected to form a polarization mode interferometer, which form a vernier effect to realize temperature and stress sensing [20].

According to the above, optical fiber sensors are mostly used to dual-parameter measurement, until now. Whereas, there are few three-parameter measurement sensors for magnetic field, temperature, and displacement. Accordingly, an optical fiber sensor is designed, which measure the three parameters of magnetic field, temperature and displacement, in this paper. Lastly, in this paper, this article mainly includes the following parts: the optical path structure of the sensor is carried out. And then, the principle analysis of the three-parameter sensing fiber structure of magnetic field, temperature and displacement. Then the experimental test of the three parameters is carried out. The sensor has the advantages of adopting a novel optical path design and realizing independent the monitoring of three parameters. It provides a solution direction for the multi-parameter influence situation caused by the magnetic field monitoring in the power system.

2. Sensing principle

2.1. Based on FBG sensing principle

It is well known that FBG can be regarded as a narrowband filter with periodic distribution, usually, FBG and FBG array are applied in magnetic field, temperature, and strain sensing [18, 21]. Moreover, narrow-band reflection of FBG is formed at a specific wavelength (Bragg wavelength) λ_b. The variation of λ_b depends on the equation (1) [22].

$$\lambda_b = 2n_{eff}\Lambda \tag{1}$$

Among them, λ_b is the pitch of the FBG, and n_{eff} is the effective refractive index of the FBG core. FBG is sensitive to temperature and strain, when temperature and strain change, the wavelength of the FBG changes as:

$$\frac{\Delta\lambda_b}{\lambda_b} = \left(1-\rho_e\right)\varepsilon_{FBG} + \left(\alpha_{FBG}+\eta\right)\Delta T \tag{2}$$

In formula (2), ρ_e is the elastic-optic coefficient, α is the thermal expansion coefficient of SiO_2, ε_{FBG} is the stress change applied to the FBG, η is the thermo-optic coefficient, and ΔT is the temperature change.

Therefore, when the temperature change is not considered, the FBG coated with GMPC is placed in a magnetic field environment, and the tensile strain exerted on the FBG by the GMPC stretching is expressed as:

$$\varepsilon = \frac{\Delta L}{L} \tag{3}$$

Here, ΔL is the change in the length of the GMPC, and L is the length of the GMPC in (3). Similarly, when the two ends of the FBG are fixed on the displacement stage, the change in the displacement will stretch the FBG, resulting in tensile strain.

2.2. Based on S-TM7-S sensing principle

In the optical fiber sensing structure, the interference spectrum is mainly generated by mode interference. Light is transmitted in an optical fiber and is mainly divided into two transmission paths, namely, transmission in the core and transmission in the cladding. SMF mainly serves the purpose of optical transmission, the light is transmitted into a seven-core fiber (MCF-7) to achieve multipath interference, subsequently. Then, it is backed to SMF. As consequence, in the process of fiber transmission, mode interference will occur between the cladding and the seven cores. Analogously, there is a mismatch in the optical path difference between the two parts. Finally, a distinct interference spectrum is produced. When the external environment changes, the interference spectrum changes [23] interference expression is followed as:

$$I = I_1 + I_2 + 2\sqrt{I_1 I_2}\phi \tag{4}$$

According to equation (4), I_1 and, I_2 are the light intensities transmitted in the core and cladding of the MCF-7, respectively. Equally, $\phi = \cos\Delta\varphi$, $\Delta\varphi$ is the phase difference between the two modes, which is showen as:

$$\Delta\varphi = \frac{2\pi\Delta n_{eff}L}{\lambda} \tag{5}$$

In equation (5), λ is the wavelength of the incident light, and Δn_{eff} is the effective refractive index difference between different interference modes of the fiber. L is the length of the MCF-7. Mode interference occurs when the optical transmission phase difference between the core and cladding modes of the fiber is $\Delta\varphi = (2K+1)\pi$. Through, the $K-th$ wavelength λ_K is expressed as equation (6):

$$\lambda_K = \frac{2n_{eff}L}{2K+1} \tag{6}$$

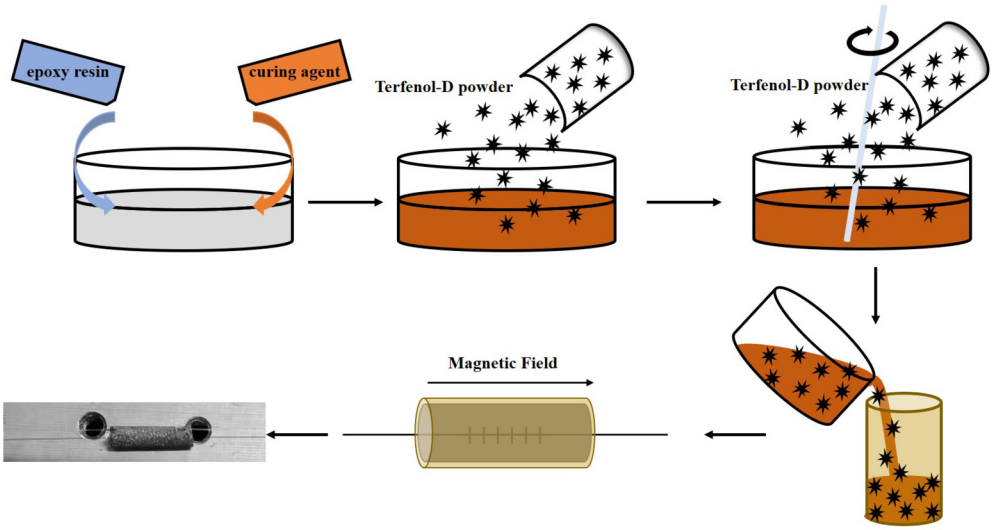

Fig. 1. The process of GMPC coated FBG.

Next, the free spectral range is followed as:

$$FSR = \lambda_{K-1} - \lambda_K = \frac{2n_{eff}}{(2K-1)(2k+1)}L \tag{7}$$

It can be seen from formula (7), L is proportional to FSR, and Δn_{eff} and L effect the value of FSR [24]. When the external environment changes, parameters are also changed such as Δn_{eff}, so the wavelength or intensity of the interference spectrum are changed. Therefore, the external environment can be monitored.

3. Experiment and result analysis based on independent measurement of three parameters

3.1. Fabrication and characterization

3.1.1. GMPC coated FBG

First, the epoxy resin and the curing agent were mixed and stirred thoroughly to form mixture A. Subsequently, the giant magnetostrictive powder (Terfenol-D powder) was introduced into Mixture A with appropriate stirring. And then, the stirred mass is introduced into the prepared mould. (Put FBG in the mold). Simultaneously, the mold was magnetized after standing for 48 hours, a GMPC material was obtained with a diameter of 6 mm and a length of 20 mm. Hence, the GMPC coated FBG was fabricated. The detailed process is shown in Fig. 1.

3.1.2. The structure of S-TM7-S

The preparation of S-TM7-S mainly includes two steps, namely: fabrication of SMF-MCF-7-SMF and taper of SMF-MCF-7-SMF.

Initially, two SMFs and a MCF-7 are removed the cladding by Miller clamps. And then, they are wiped using alcohol to clean up the residual cladding. Afterwards, the end faces of them are cut and flattened by fiber cleaver, respectively. Then, an SMF with a neat end face and a MCF-7 is placed on the two ports of the fiber fusion splicer for fusion splicing. Next, put the end face of the spliced structure with the seven-core fiber into one port of the fusion splicer, and put another single-mode fiber into the other port, and splicing to form the SMF-MCF-7-SMF structure. The structure of SMF-MCF-7-SMF is showed as Fig. 2(a). Apparently, the fixed lengths of MCF-7 are controlled to be 15 mm, 20 mm, and 25 mm, respectively.

Secondly, the MCF-7 of SMF-MCF-7-SMF is tapered on Hydrogen-oxygen flame cone drawing machine to form the structure of S-TM7-S. In detail, first Hydrogen-oxygen flame cone drawing machine is opened, then the MCF-7 of the SMF-MCF-7-SMF is placed in the middle of the flame of Hydrogen-oxygen flame cone drawing machine. Immediately after, the taper platform is operated to draw the taper to form the S-TM7-S structure. Last, the structure of S-TM7-S is packaged on the packaging table, which is exhibited as Fig. 2(b). Indeed, the length of the taper is between 8.40 mm and 8.50 mm in this experiment.

3.2. Experimental details

Fig. 3 is shown as a three-parameter sensor measurement device. The light from the ASE is transmitted to a 1:3 coupler. The three ports of this coupler are connected to circulator 1, circulator 2 and the structure of S-TM7-S, respectively.

Among, the circulator 1 which is connected to GMPC coated FBG1, which is used to measure magnetic field. Equally, the circulator 2 is attach to FBG2, which is applied to micro-displacement. The structure of S-TM7-S realizes temperature monitoring. Lastly, the respective connection of three ports is realized through the WDM, the output the measured spectrum to the OSA. In this way, three sensing units can be individually connected to WDM, the independent testing of the three parameters can be realized.

3.3. Result analysis

3.3.1. Based on magnetic field sensing analysis

Finite Element Method (FEM) simulation analysis In this paper, two prototypes of Terfenol-D material are performed on FEM simulations, namely cuboid and cylinder. Meanwhile, the magnetostrictive properties of materials are studied with the same shape and different lengths. The purpose is achieved best compromise between minimal Terfenol-D material and higher magnetic field sensitivity. The simulation uses the coupling of the AC/DC and Solid Mechanics Modules in the COMSOL Multiphysics™ to run Terfenol-D material tests in three dimensions (3D) under a steady state magnetic field (mf). 3D space is applied with a magnetic field obtained by Ampere's law, which is followed as:

$$B = \mu_0 \mu_r H + B_r \tag{8}$$

At this time, μ_0 is the magnetic permeability in the space, μ_r is the relative magnetic permeability, B is the magnetic flux density and B_r is the residual magnetic flux density among of formula (8). Intriguingly, the Terfenol-D of μ_r is equal to 5 [25]. Equally, a stable, uniform magnetic field is applied along the Z axial direction to study the magnetic flux density distribution of the material. The FEM simulation is shown as Fig. 4 about Terfenol-D material of different shape.

Above, it can be seen that two models have the same height, and diameter. When a magnetic field is applied, the magnetostrictive effect

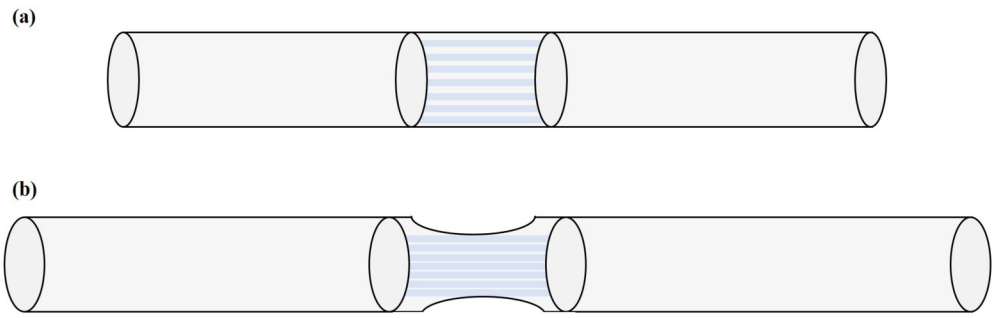

Fig. 2. (a) The structure of SMF-MCF7-SMF. (b) The structure of S-TM7-S.

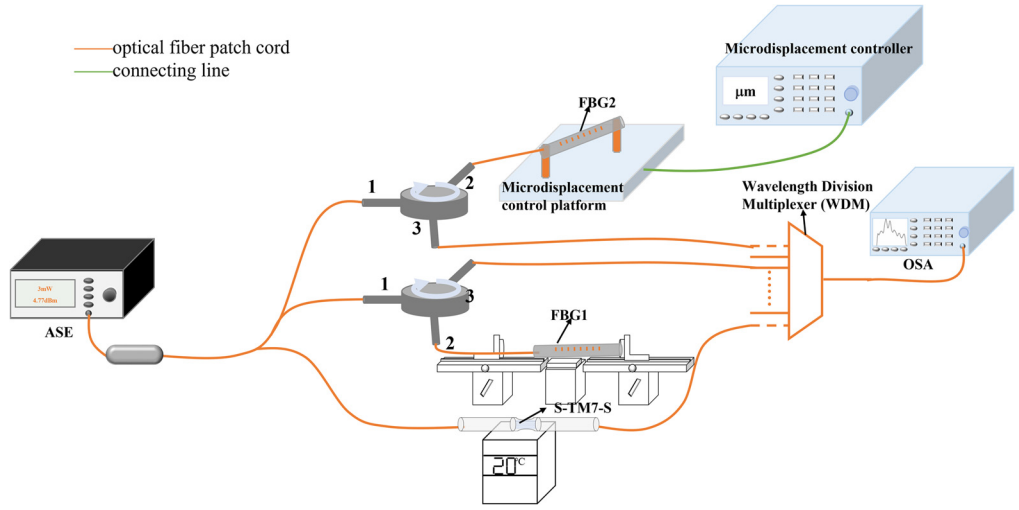

Fig. 3. Three-parameter sensor measurement device.

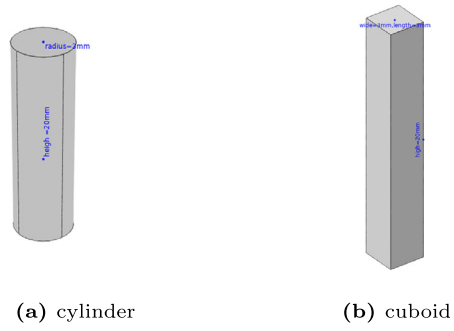

Fig. 4. The FEM simulation model: (a) cylinder, (b) cuboid. (Note: The red arrow indicates the direction of the magnetic field).

curves of the two different shapes of materials with increasing magnetic field are shown in Fig. 5. It can be seen that when the Terfenol-D material does not reach saturation, the magnetostriction performance of the cuboid is better than that of the cylinder as the magnetic field increases, while its saturation magnetostriction coefficient is approximated when saturation is reached. In addition, when under low magnetic field conditions (< 1000 Oe), the magnetostriction produced by both shapes of the material is basically the same. While when the magnetostriction effect of the material is in the linear region, the slope of the magnetostriction curve (k) of the cuboid is larger than that of the cylinder, and the linearity (R^2) is lower than that of the cylinder, as shown in Fig. 5. Thus, a comprehensive consideration of linearity and sensitivity (i.e. slope), as well as the same diameter and height, requires far more Terfenol-D powder for a cuboid than a cylinder.

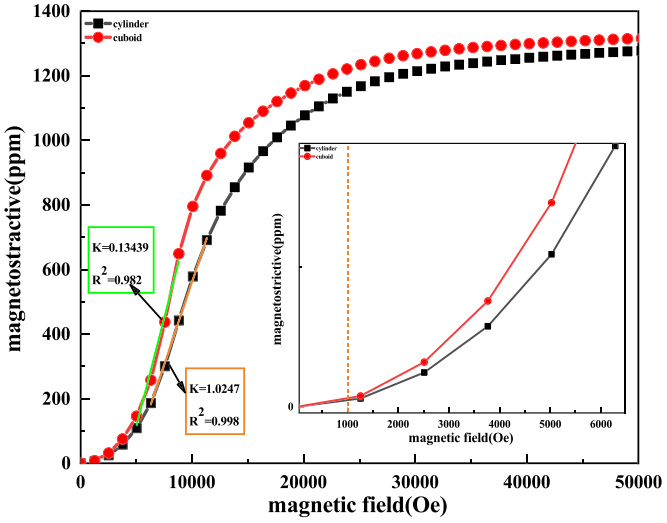

Fig. 5. Magnetostrictive effect after applying the magnetic field regarding Terfenol-D material. (Note: 1mT = 10Oe.)

Accordingly, Since the magnetic field is measured in the range of 0 mT-60 mT (i.e. 0 Oe-600 Oe) and in the consideration of linearity, the cylinder is applied as making model GMPC, which is measured magnetic field.

The experimental measuring about magnetic field It is showed that the sensitivity of the cuboid Terfenol-D material is -1.63 pm/mT, which is obviously lower than the sensitivity of the cylinder Terfenol-D material

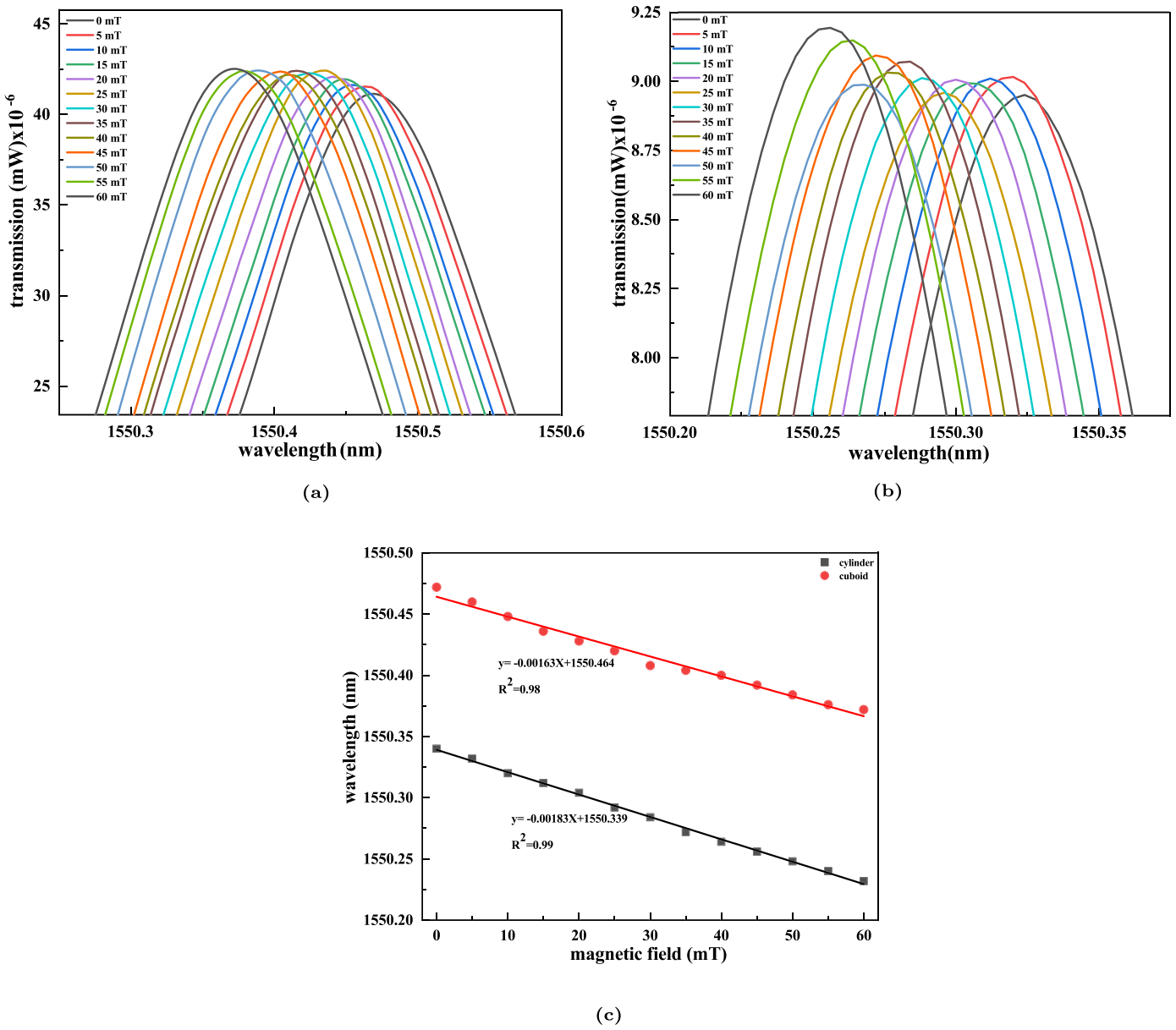

Fig. 6. The different shape Terfenol-D material is measured in magnetic field: (a) the optical spectrum of cuboid, (b) the optical spectrum of cylinder;(c) the linear fit.

-1.83 pm/mT, in measured range of 0 mT-60 mT (Fig. 6). This may, in a real experimental setting, produce such a phenomenon due to the higher linearity of the cylinder Terfenol-D material.

Then, the solidification model of the GMPC material adopts a cylindrical shape. In this experiment, we prepared the GMPC coated FBG sensing unit as shown in Fig. 1. Simultaneously, it is investigated effect respecting the ratio of Terfenol-D powder and mixture A on the magnetic field measurements. Notably, the Terfenol-D powder: mixture A is equal to 5:1, 7.5:1, 10:1, respectively. From Fig. 7, it can be observed the GMPC magnetic field detection results. Overall, the optical spectrum is blue-shifts, as the magnetic field increases.

In detail, when Terfenol-D powder: mixture A is equal to 5:1 in GMPC material, the magnetic field detection step size is larger (10 mT) (Fig. 7(a)), and the detection sensitivity is -0.307 pm/mT. In contrast, when Terfenol-D powder: mixture A is 7.5:1 (Fig. 7(b)) and 10:1 (Fig. 7(c)), the detection sensitivity of the material is -1.2 pm/mT and -1.7 pm/mT, respectively, which is significantly higher than that the ratio of the material is 5:1 (Fig. 7(d)). Equally, the magnetic field detection step size is 5 mT, which is obviously reduced. As consequence, with the increase of the proportion of Terfenol-D powder in GMPC materials, the detection sensitivity was visibly improved. Meanwhile, compared with the same volume of bulk Terfenol-D material, GMPC material greatly saves rare metal material.

3.3.2. Based on temperature sensing analysis

Fig. 8 (a), (b), and (c) show the temperature sensitivity results of S-TM7-S for seven core fiber lengths of 15 mm, 20 mm, and 25 mm, respectively. The lower limit of temperature detection is 60 °C and the upper limit is 100 °C. The valley is selected as the indicator in the range of 1543 nm to 1547 nm, which can be seen that with temperature increasing, the spectrum, the different length of seven core fiber in S-TM7-S, are red-shift. Moreover, linear fit plot is shown as Fig. 9, which shows that the sensitivity of S-TM7-S is enhanced as the length of the seven-core fiber increases. When the length of seven-core fiber is 25 mm, the highest temperature sensitivity is 29.93 pm/°C.

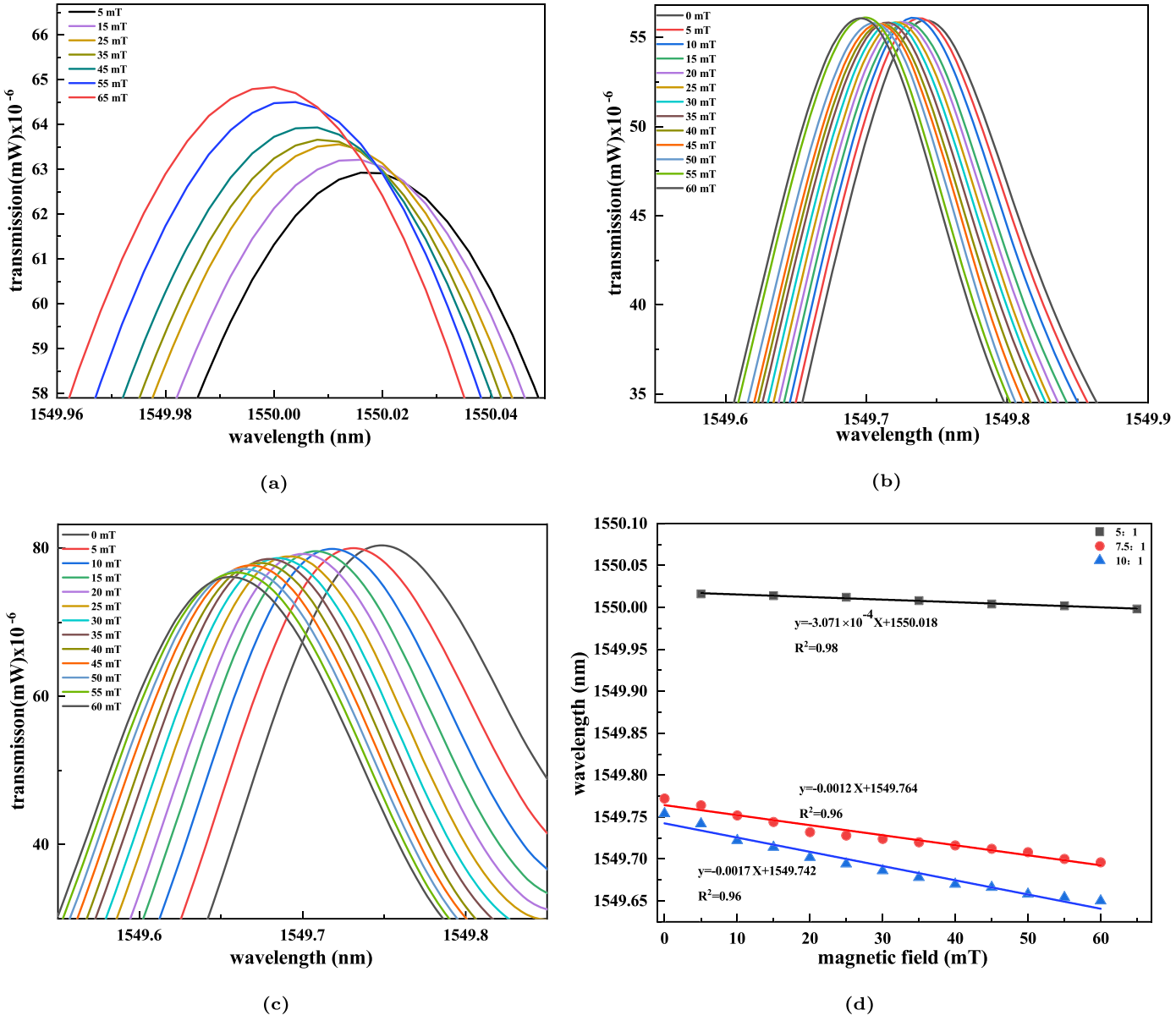

Fig. 7. Results of magnetic field measurements using different concentrations of GMPC: (a) measured optical spectrum about the Terfenol-D powder: mixture A is equal to 5:1, (b) measured optical spectrum about the Terfenol-D powder: mixture A is equal to 7.5:1, (c) measured optical spectrum about the Terfenol-D powder: mixture A is equal to 10:1, (d) linear fit.

3.3.3. Based on displacement sensing analysis

The displacement sensing platform is shown in Fig. 3. FBG2 is used to measure displacement, the displacement is measured from 0 μm to 95 μm. Additionally, the detection step is 5 μ m. As the displacement increases, the wavelength of FBG2 is blue-shifted (Fig. 10). After linear fitting, it is found that the linear sensitivity is -1.18 pm/μm, which the range of displacement is from 0 μm to 95 μm (Fig. 11). Intriguingly, in the range of 0 μm to 30 μm, the linear sensitivity is higher at -1.51 pm/μm.

4. Experiments and results analysis based on simultaneous measurement of three parameters

Based on the above experimental results, a seven-core fiber length of 25 mm in a S-TM7-S was cascaded to the FBG (S-TM7-S-FBG), and the FBG was clad with GMPC materials of 10:1. The structure, S-TM7-S-FBG, is used for three-parameter detection of magnetic field, temperature and displacement. A straight-through optical path is used for detection, as shown in Fig. 12. The transmission spectrum of the sensing unit is shown in Fig. 13, and we use the wave valley dipA, dipB, and FBG for the three parameters, respectively.

In order to measure the magnetic field, the sensing unit is placed in a magnetic field environment and the sensing spectrum is observed between 20 mT and 45 mT range. It can be showed that when the magnetic field is enhanced, the wave valleys dipA and dipB of S-TM7-S drift insignificantly, as shown in Fig. 14(a) and 14(b), respectively. In addition, the FBG is a blue shift (Fig. 14(c)). From the linear fit results, it is clear that the sensor consists of good linearity and the sensitivity of FBG($K_{M,FBG}$) is -1.2 pm/mT (Fig. 14(d)). However, the sensitivities of dipA and dipB are two orders of magnitude smaller than the FBG sensitivity, which can be ignored.

Then, the sensing unit is placed on the temperature control console for temperature measurement. The temperature varied between 60 °C and 100 °C in steps of 5 °C. The dipA, dipB and FBG wavelength shifts were 0.5036 nm, 1.1348 nm, and 0.4728 nm, respectively (Fig. 15(a), (b), (c)). The linear fit indicates that the temperature sensitivity of dipA,

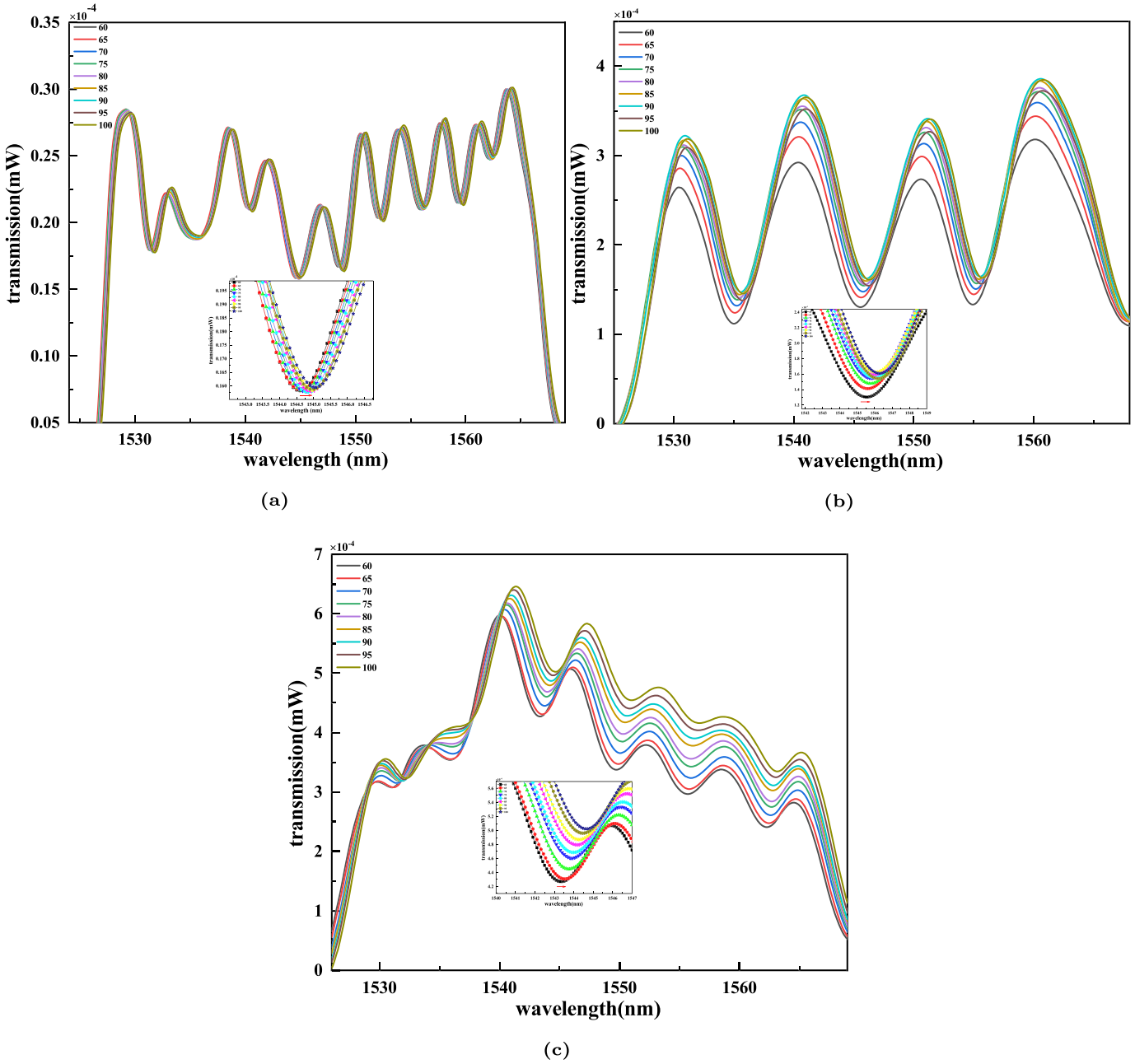

Fig. 8. Temperature measurement optical spectrum of the S-TM7-S: (a) seven-core optical fibers with lengths of 15 mm, (b) seven-core optical fibers with lengths of 20 mm, (c) seven-core optical fibers with lengths of 25 mm.

dipB, and FBG are $K_{(T,dipA)}$ = 12.59 pm/°C, $K_{(T,dipA)}$ = 28.37 pm/°C, $K_{(T,dipA)}$ = 11.82 pm/°C, separately (Fig. 15(d)).

In the following, the sensing unit is placed on the displacement stage, which is activated to observe the spectral change of the displacement from 0 μm to 40 μm. Fig. 16(a), (b), and (c) show the transmission spectra of dipA and dipB of S-TM7-S, and FBG, respectively. The linear fit of the measurement results is shown in Fig. 16(d). By fitting the results, it can be seen that the displacement sensitivity of dipA, dipB, and FBG are $K_{(\epsilon,dipA)} = 11.7$ pm/μm, $K_{(\epsilon,dipB)} = 2.02$ pm/μm, and $K_{(\epsilon,FBG)} = -1.6$ pm/μm, respectively.

When the magnetic field, temperature, and displacement is changed simultaneously, the wavelength shifts of dipA, dipB, and FBG can be expressed in a matrix (9) as follows.

$$\begin{bmatrix} \Delta\lambda_{dipA} \\ \Delta\lambda_{dipB} \\ \Delta\lambda_{FBG} \end{bmatrix} = \begin{bmatrix} K_{(M,dipA)}, K_{(\epsilon,dipA)}, K_{(T,dipA)} \\ K_{(M,dipA)}, K_{(\epsilon,dipB)}, K_{(T,dipB)} \\ K_{(M,dipA)}, K_{(\epsilon,FBG)}, K_{(T,FBG)} \end{bmatrix} \begin{bmatrix} \Delta M \\ \Delta\epsilon \\ \Delta T \end{bmatrix} \tag{9}$$

Where $\Delta\lambda_{dipA}$, $\Delta\lambda_{dipB}$, and $\Delta\lambda_{FBG}$ represents dipA, dipB and FBG drift amount respectively. Besides, K_M, K_ϵ, and K_T are showed the sensitivity of magnetic field, displacement, and temperature, so, which the sensitivity is obtained as formula (10):

$$\begin{bmatrix} \Delta M \\ \Delta\epsilon \\ \Delta T \end{bmatrix} = \begin{bmatrix} K_{(M,dipA)}, K_{(\epsilon,dipA)}, K_{(T,dipA)} \\ K_{(M,dipA)}, K_{(\epsilon,dipB)}, K_{(T,dipB)} \\ K_{(M,dipA)}, K_{(\epsilon,FBG)}, K_{(T,FBG)} \end{bmatrix}^{-1} \begin{bmatrix} \Delta\lambda_{dipA} \\ \Delta\lambda_{dipB} \\ \Delta\lambda_{FBG} \end{bmatrix} \tag{10}$$

According to matrix (10), the magnetic field, displacement, and temperature sensitivity of the sensing unit can be calculated. Therefore, it is achieved about simultaneous measurement of the three parameters.

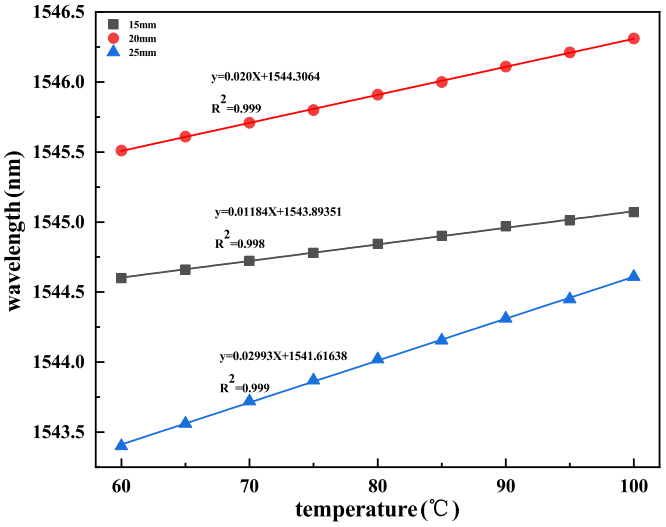

Fig. 9. The total linear fit plot about the seven-core fiber of 15 mm, 20 mm, 25 mm, respectively.

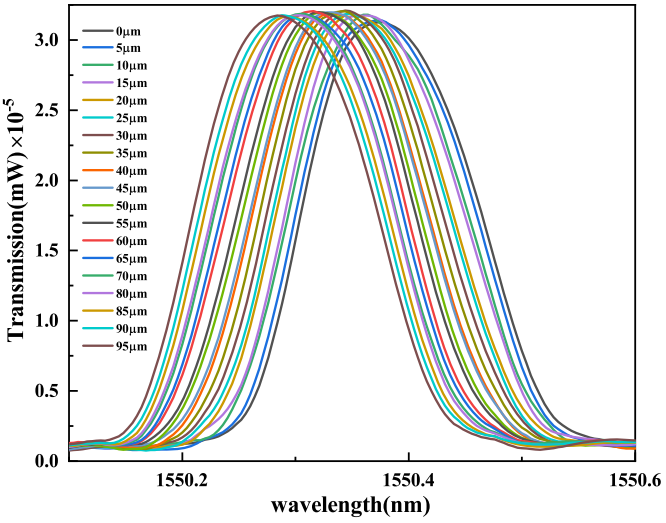

Fig. 10. The optical spectrum of displacement sensing.

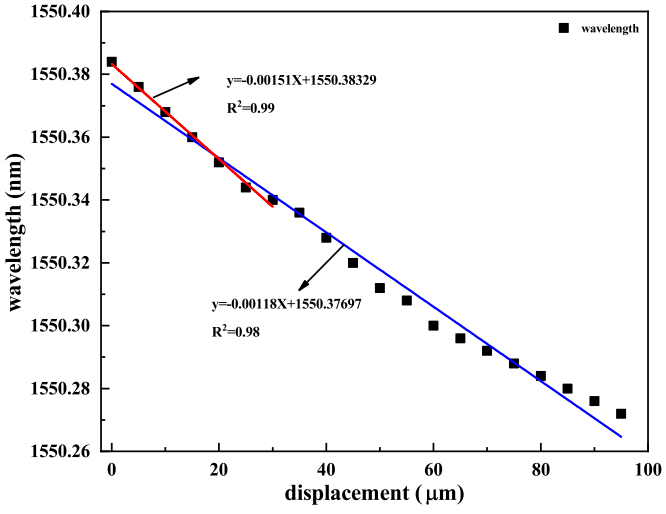

Fig. 11. The displacement measuring of linear fit plot.

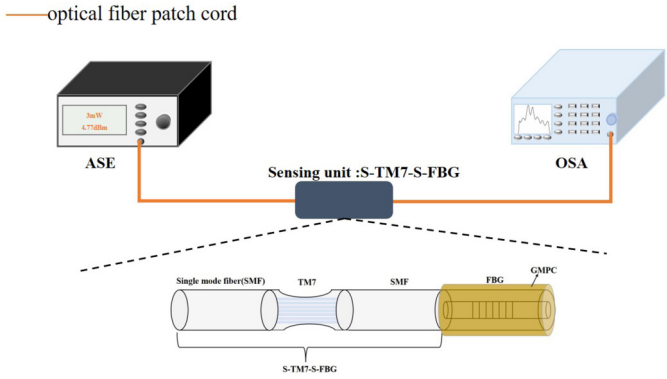

Fig. 12. Straight-through optical path.

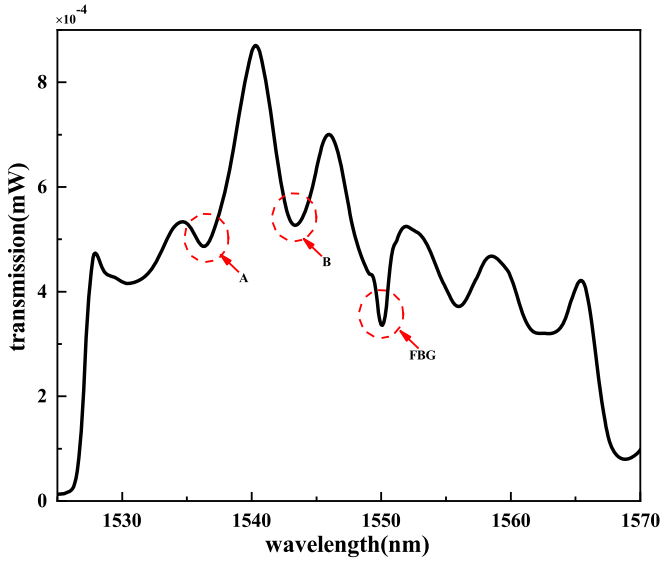

Fig. 13. Measured transmission spectrum of the sensor.

In order to test the repeatability of the sensing unit, three similar sensing units were repeatedly made. First, the S-TM7-S structural parameters were kept consistent, further, the FBG with the same parameters was used. There is no significant variation in the transmission spectra of the three sensing units. Then, their spectral errors are extremely low, which indicates the good repeatability and reproducibility of the sensing units (Fig. 17). Besides, the detection of proposed magnetic field, displacement and temperature can be applied to the health monitoring of high-voltage lines and others in the field of electrical engineering. It is demonstrated that most of the fiber optic sensors in recent years are based on two-parameter measurements and less on three-parameter measurements in Table 1.

Moreover, as far as temperature sensing is concerned, the sensing unit used in this paper is not coated with a sensitive material, but the temperature detection sensitivity can be up to 28.37 pm/°C. Although the sensitivity of magnetic field sensing is lower compared to [26], however, the sensing unit is simple, convenient, and durable in this paper.

5. Conclusion

In this paper, an optical fiber sensor is proposed, which is realized three-parameter measurement. Moreover, a novel optical path construction method is adopted. Firstly, the independent measurement of three parameters was carried out experimentally, and the optimal measure-

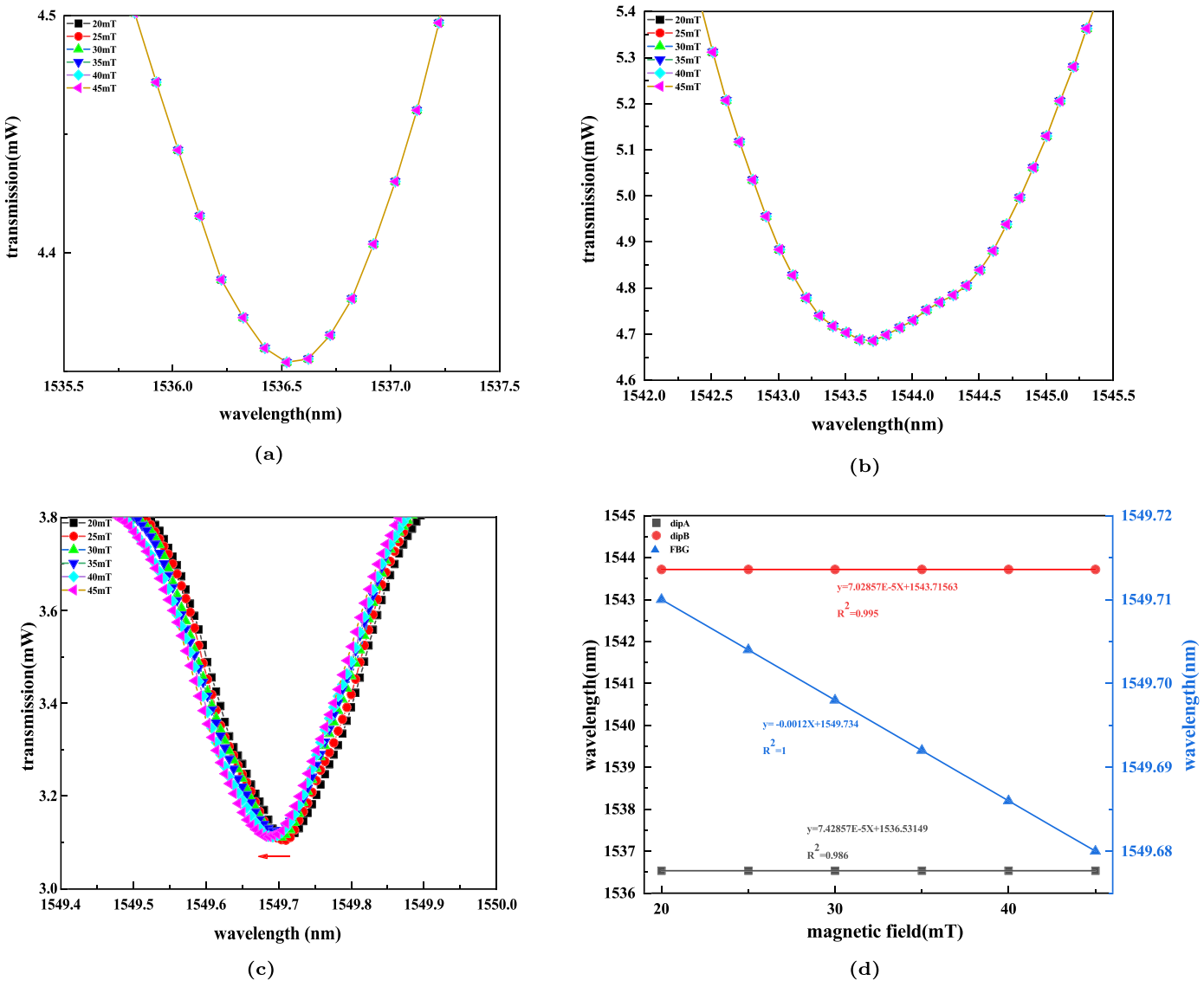

Fig. 14. The result of measured the magnetic field based on S-TM7-S-FBG: (a) measured optical spectrum about dipA, (b) measured optical spectrum about dipB, (c) measured optical spectrum about FBG, (d) linear fit.

ment parameters of the independent measurement were selected for making the three-parameter simultaneous measurement structure (i.e., S-TM7-S-FBG). Finally, the simultaneous detection of three parameters was achieved and detuned using the matrix method. Consequently, the optical fiber sensor can not only realize three-parameter measurement, but also has the advantages of convenient measurement and material saving. Lastly, the sensor can be used in power systems, biological monitoring, aerospace monitoring and other fields. In particular, it provides directions for implementing multiparameter detection in complex power systems.

Declarations

Author contribution statement

Chi Liu: Conceived and designed the experiments; Performed the experiments; Analyzed and interpreted the data; Contributed reagents, materials, analysis tools or data; Wrote the paper. Yue Feng: Conceived and designed the experiments; Performed the experiments. Xin Liu: Conceived and designed the experiments; Contributed reagents, materials, analysis tools or data. Yunqiang Li: Analyzed and interpreted the data; Wrote the paper. Tao Shen: Conceived and designed the experiments; Analyzed and interpreted the data; Contributed reagents, materials, analysis tools or data.

Funding statement

This work was supported by National Natural Science Foundation of China [52102164].

Data availability statement

Data will be made available on request.

Declaration of interests statement

The authors declare no conflict of interest.

Additional information

No additional information is available for this paper.

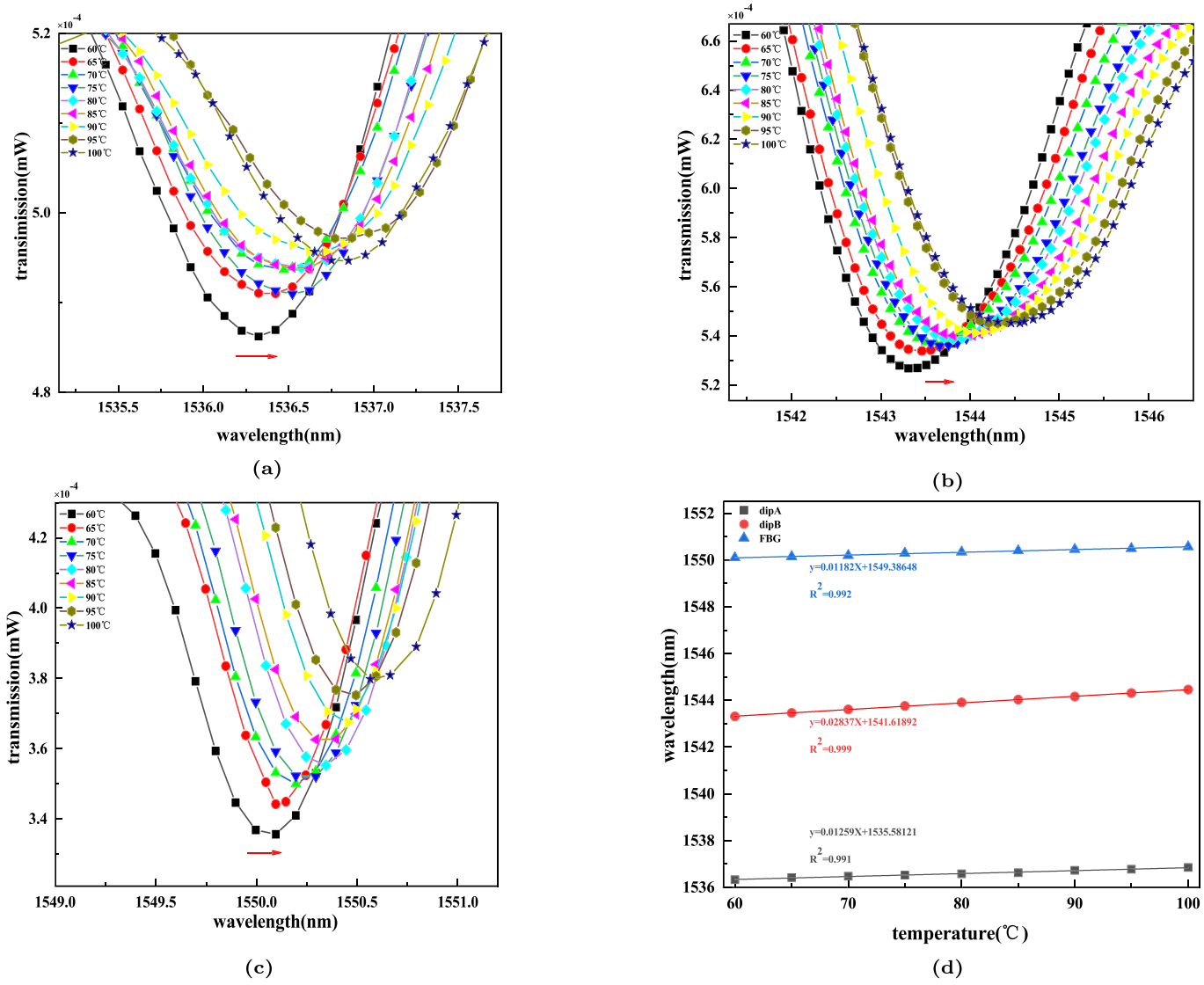

Fig. 15. The result of measured the temperature based on S-TM7-S-FBG: (a) measured optical spectrum about dipA, (b) measured optical spectrum about dipB, (c) measured optical spectrum about FBG, (d) linear fit.

Table 1. Comparison of this work with others.

publication year	the structure of optical fiber	number of parameters	measurement parameters/ sensitivity
2017 [13]	FMF + spherical structure[1]	2	temperature(T)/(Max)0.05 nm/°C, refective index (RI)/ (Max)-48.82 nm/RIU
2018 [16]	FP + FBG[2]	2	T/(Max)7.82 pm/°C, strain(N)/(Max)2.1 pm/$\mu\varepsilon$
2019 [17]	offset spliced with SMF-FMF-FBG	2	T/(Max)-34.3 pm/°C, stress(S)/(Max)-2 pm/$\mu\varepsilon$
2021 [25]	FBG coated Terfenol-D composite material	1	magnetic field(H)/ (conical)1.7 pm/mT
2021 [26]	NTF cascaded FBG[3]	2	H/(Max)1.159 nm/mT, T/(Max)-1.737 nm/°C
2022 [27]	SNFNS[4]	3	T/(Max)0.0095 nm/°C, humidity/(Max)0.034 nm/%RH, RI/(Max)134.17 nm/RIU
this work	S-TM7-S-FBG	3	T/(Max)28.37 pm/°C, displacement/(Max)2.02 pm μm, H/(Max)-1.2 pm/mT

Note: [1] FMF-Few Mode Fiber, [2] FP-Fiber optic Fabry-Perot Cavity, [3] NTF-Nonadiabatic Tapered Micro-fiber, [4] SNFNS: SMF-NCF-FMF-NCF-SMF (NCF-No Core Fiber).

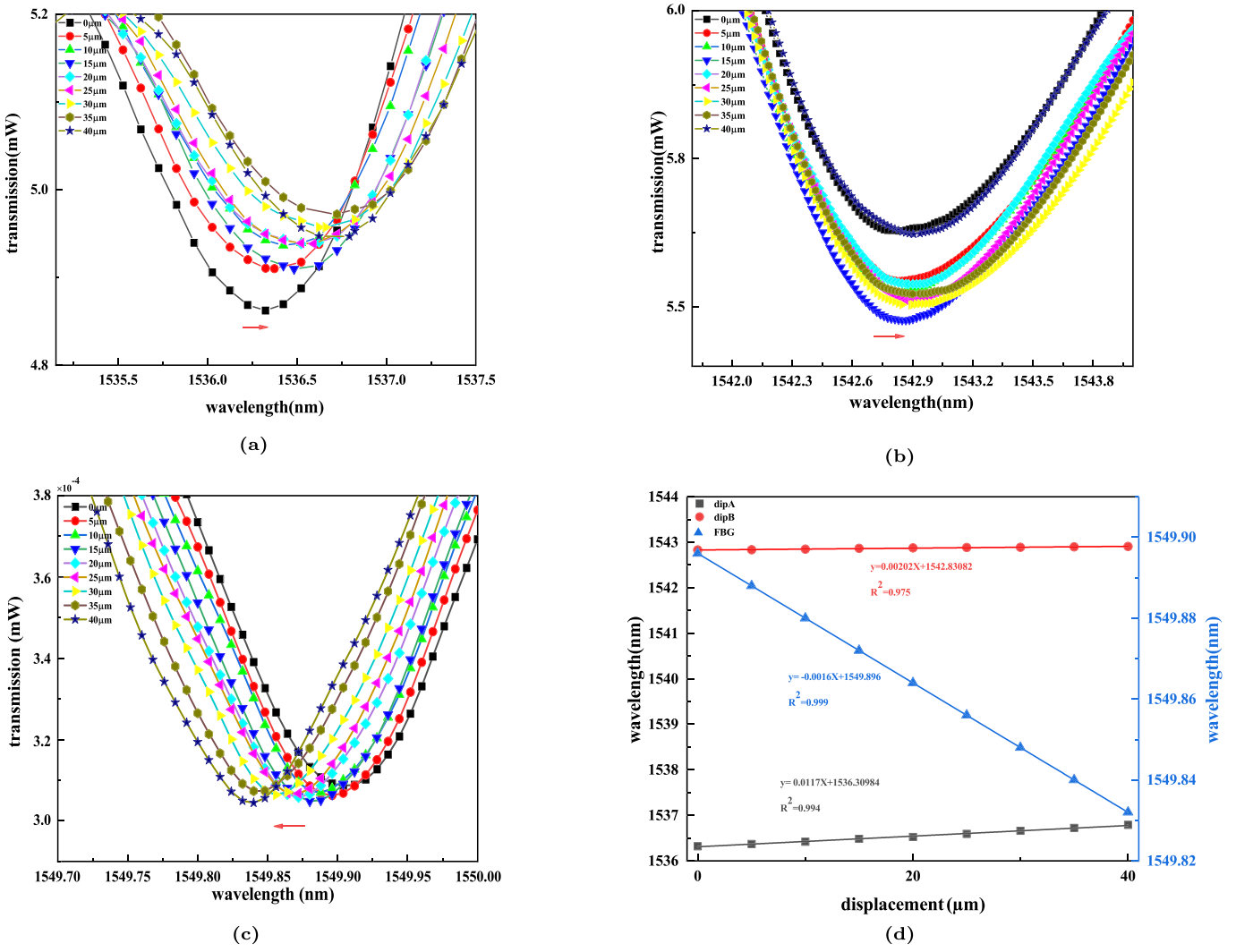

Fig. 16. The result of measured the displacement based on S-TM7-S-FBG: (a) measured optical spectrum about dipA, (b) measured optical spectrum about dipB, (c) measured optical spectrum about FBG, (d) linear fit.

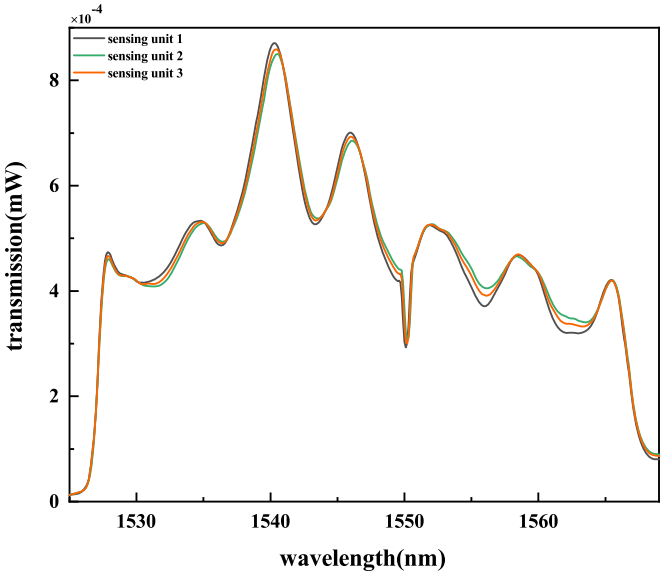

Fig. 17. Repeatable production of sensing units.

References

[1] K.C. Kao, G.A. Hockham, Dielectric-Fibre Surface Waveguides for Optical Frequencies, Proceedings of the Institution of Electrical Engineers, vol. 113, IET, 1966, pp. 1151–1158.

[2] F. Kapron, D.B. Keck, R.D. Maurer, Radiation losses in glass optical waveguides, Appl. Phys. Lett. 17 (10) (1970) 423–425.

[3] D. Keck, R. Maurer, P. Schultz, On the ultimate lower limit of attenuation in glass optical waveguides, Appl. Phys. Lett. 22 (7) (1973) 307–309.

[4] L. Zhu, N. Zhao, Q. Lin, L. Zhao, Z. Jiang, Optical fiber spr magnetic field sensor based on photonic crystal fiber with the magnetic fluid as cladding, Meas. Sci. Technol. 32 (7) (2021) 075106.

[5] Y. Sun, T. Lu, Y. Moreno, L. Li, H. Wang, K. Zhou, Q. Sun, D. Liu, Z. Yan, L. Zhang, Theoretical and experimental analysis of the directional ri sensing property of tilted fiber grating, J. Lightwave Technol. 39 (2) (2021) 674–681.

[6] X. Jia, X. Zhou, M. Bi, G. Yang, M. Hu, T. Wang, High-sensitivity optical fiber temperature sensor of cascaded fsi and mzi based on vernier effect, Opt. Fiber Technol. 65 (2021) 102625.

[7] Y. Deng, Q. Liu, Z. He, Distributed fiber-optic acoustic sensor for sparse-wideband vibration sensing with time delay sampling, IEEE Sens. J. 21 (12) (2021) 13290–13295.

[8] P. Zhu, X. Xie, X. Sun, M.A. Soto, Distributed modular temperature-strain sensor based on optical fiber embedded in laminated composites, Composites, Part B, Eng. 168 (2019) 267–273.

[9] G.-M. Ma, H.-y. Zhou, M. Zhang, C.-R. Li, Y. Yin, Y.-Y. Wu, A high sensitivity optical fiber sensor for gis partial discharge detection, IEEE Sens. J. 19 (20) (2019) 9235–9243.

[10] K. Sroka, D. Złotecka, The risk of large blackout failures in power systems, Arch. Elektrotech. (2019) 411–426.

[11] Q. Liu, Y. Jiang, Y. Sun, C. Hu, J. Sun, C. Liu, J. Lv, J. Zhao, Z. Yi, P.K. Chu, Surface plasmon resonance sensor based on u-shaped photonic quasi-crystal fiber, Appl. Opt. 60 (6) (2021) 1761–1766.
[12] A. Leal-Junior, C. Díaz, A. Frizera, H. Lee, K. Nakamura, Y. Mizuno, C. Marques, Highly sensitive fiber-optic intrinsic electromagnetic field sensing, Adv. Photon. Res. 2 (1) (2021) 2000078.
[13] Z. Tong, X. Wang, Y. Wang, W. Zhang, M. Gong, Dual-parameter optical fiber sensor based on few-mode fiber and spherical structure, Opt. Commun. 405 (2017) 60–65.
[14] Z. Yong, C. Lu, L. Xue-Gang, L. Ri-Qing, A modal interferometer based on single mode fiber-hollow core fiber-single mode fiber structure filled with alcohol and magnetic fluid for simultaneously measuring magnetic field and temperature, Acta Physica Sinica 66 (7) (2017) 070601.
[15] C. Li, T. Ning, J. Li, L. Pei, C. Zhang, C. Zhang, H. Lin, X. Wen, Simultaneous measurement of refractive index, strain, and temperature based on a four-core fiber combined with a fiber Bragg grating, Opt. Laser Technol. 90 (2017) 179–184.
[16] X. Zhang, W. Peng, L.-Y. Shao, W. Pan, L. Yan, Strain and temperature discrimination by using temperature-independent fpi and fbg, Sens. Actuators A, Phys. 272 (2018) 134–138.
[17] X. Gao, T. Ning, C. Zhang, J. Xu, J. Zheng, H. Lin, J. Li, L. Pei, H. You, A dual-parameter fiber sensor based on few-mode fiber and fiber Bragg grating for strain and temperature sensing, Opt. Commun. 454 (2020) 124441.
[18] A.G. Leal-Junior, V. Campos, C. Díaz, R.M. Andrade, A. Frizera, C. Marques, A machine learning approach for simultaneous measurement of magnetic field position and intensity with fiber Bragg grating and magnetorheological fluid, Opt. Fiber Technol. 56 (2020) 102184.
[19] B. Zhan, T. Ning, L. Pei, J. Li, L. Liu, X. Gao, J. Xu, J. Zheng, J. Wang, B. Ai, Terfenol-D based magnetic field sensor with temperature independence incorporating dual fiber Bragg gratings structure, IEEE Access 9 (2021) 32713–32720.
[20] W. Zhang, X. Wu, C. Zuo, L. Gui, J. Shi, X. Zhao, S. Mu, J. Liu, B. Yu, Highly sensitive temperature and strain sensor based on fiber Sagnac interferometer with vernier effect, Opt. Commun. 506 (2022) 127543.
[21] A.G. Leal-Junior, A. Frizera, A. Theodosiou, C. Díaz, M. Jimenez, R. Min, M.J. Pontes, K. Kalli, C. Marques, Plane-by-plane written, low-loss polymer optical fiber Bragg grating arrays for multiparameter sensing in a smart Walker, IEEE Sens. J. 19 (20) (2019) 9221–9228.
[22] H. Pei, J. Jing, S. Zhang, Experimental study on a new fbg-based and terfenol-d inclinometer for slope displacement monitoring, Measurement 151 (2020) 107172.
[23] W. Bao, N. Sahoo, Z. Sun, C. Wang, S. Liu, Y. Wang, L. Zhang, Selective fiber Bragg grating inscription in four-core fiber for two-dimension vector bending sensing, Opt. Express 28 (18) (2020) 26461–26469.
[24] R. Yang, L. Zhu, J. Li, T. Xu, G. Sun, High fringe visibility Mach-Zehnder interferometric sensor based on a four-core fiber, Instrum. Sci. Technol. 48 (3) (2020) 326–337.
[25] J.D. Lopez, A. Dante, C.C. Carvalho, R.C. Allil, M.M. Werneck, Simulation and experimental study of fbg-based magnetic field sensors with terfenol-d composites in different geometric shapes, Measurement 172 (2021) 108893.
[26] Y. Zhang, S. Pu, Y. Li, Z. Hao, D. Li, S. Yan, M. Yuan, C. Zhang, Magnetic field and temperature dual-parameter sensor based on nonadiabatic tapered microfiber cascaded with fbg, IEEE Access 10 (2022) 15478–15486.
[27] M. Wu, W. Zhang, Z. Tong, X. Wang, Y. Zhao, J. Zhang, G. Yan, Mach-Zehnder interferometer for multi-parameter measurement sensor based on smf-ncf-fmf-ncf-smf, Optik 249 (2022) 168227.